Title	Ultrasonic diffraction from a transducer with arbitrary geometry and strength distribution
Author(s)	Ogi, Hirotsugu; Hirao, Masahiko; Honda, Takashi et al.
Citation	Journal of the Acoustical Society of America. 1995, 98(2), p. 1191-1198
Version Type	VoR
URL	https://hdl.handle.net/11094/84149
rights	Copyright 1995 Acoustical Society of America. This article may be downloaded for personal use only. Any other use requires prior permission of the author and the Acoustical Society of America.
Note	

Ultrasonic diffraction from a transducer with arbitrary geometry and strength distribution

Hirotsugu Ogi, Masahiko Hirao, and Takashi Honda
Faculty of Engineering Science, Osaka University, Toyonaka Osaka 560, Japan

Hidekazu Fukuoka
Nara National College of Technology, Yamatokoriyama, Nara 639-11, Japan

The exact solution to the Helmholtz equation with a Dirichlet boundary condition is obtained to study three-dimensional ultrasonic diffraction phenomena and derive the numerical data of amplitude loss and the phase shift for correcting induced errors. Calculation is made for near-field diffraction, for the rectangular transducers, and for the transducers with strength distribution on the radiating area. In the near field, where the wavelength and the propagation distance are comparable with each other, the longitudinal and shear waves undergo different diffraction. For transducers having a noncircular shape and a strength distribution on the area, both the amplitude loss and the phase shift experience different tendencies from the classical work on the circular piston source. Use of diffraction data specific to each measurement condition is then necessary to correct the errors. The calculated results are verified for pulse-echo measurements using a shear-wave electromagnetic acoustic transducer. © 1995 Acoustical Society of America.

PACS numbers: 43.20.Fn, 43.20.Gp, 43.20.Rz

INTRODUCTION

An ultrasonic beam radiated from a finite source spreads laterally during the propagation in the medium, depending on the frequency, the transducer size, and the propagated distance. A part of the incident wave energy fails to return to the transducer aperture, causing amplitude loss and phase shift in pulse-echo measurements. We must appropriately remove the involved errors for accurate velocity and attenuation measurements. This phenomena, known as diffraction, has been investigated by many authors.[1-8] Seki *et al.*[1] studied the effect for a longitudinal wave from a circular piston transducer into an isotropic homogeneous material. They gave the features for use in correcting the diffraction errors. Following them, Papadakis[4,5] derived the diffraction character in an anisotropic material. Beissner[6] calculated the effect of the difference of radii of the sending and receiving areas. Tang *et al.*[7] performed a numerical simulation for the diffraction of longitudinal and shear waves from a circular piston source in any frequency region.

Most existing work has been focused on the problem of the ultrasonic wave generated by a circular source with a uniform strength over it, being based on Rayleigh's approximate expression.[8] We start with the exact solutions to the Helmholz equation with a Dirichlet boundary condition for both longitudinal and shear waves to account for their near-field behavior. This paper further expands the diffraction analysis to accommodate the practical cases such as a noncircular shape and a strength distribution on the area. These situations are often encountered with the use of electromagnetic acoustic transducers (EMATs) and laser ablation excitations. Numerical calculation emphasizes the necessity of using the correction data specific to each measuring configuration. To illustrate the usefulness, we apply the numerical result for correcting the attenuation measurement with a shear-wave EMAT. The EMAT relies on the Lorentz force mechanism and operates with a rectangular source area on the sample surface and a strength distribution over it. After some simplifications, we calculate the amplitude loss for the multiple echoes and compare with the pulse-echo experiments using the rf bursts and a steel plate as a sample. The calculation shows a good agreement with the experiments, verifying the present analysis.

I. THEORY OF DIFFRACTION PHENOMENA

A. Potential field

In a homogeneous isotropic elastic material with no external force acting, the equation of motion in terms of the displacement $\mathbf{u}(\mathbf{x},t)$ is decomposed to the Helmholtz equations

$$\nabla^2 \phi + k_L^2 \ddot{\phi} = 0 \quad [k_L = \omega/C_L, \quad C_L^2 = (\lambda + 2\mu)/\rho], \quad (1)$$

$$\nabla^2 \boldsymbol{\psi} + k_T^2 \ddot{\boldsymbol{\psi}} = 0 \quad (k_T = \omega/C_T, \quad C_T^2 = \mu/\rho), \quad (2)$$

by use of the scalar potential ϕ and the vector potential $\boldsymbol{\psi}$, satisfying[9]

$$\mathbf{u} = \text{grad } \phi + \text{rot } \boldsymbol{\psi}. \quad (3)$$

Here, λ and μ are the elastic constants (Lamé constants), ω is the frequency, ρ is the density of the medium, k is the wave number, and C is the ultrasonic velocity. The suffix L or T indicates a longitudinal wave or a shear wave.

We first consider a longitudinal wave ($\boldsymbol{\psi}=0$). In Fig. 1, a sending plane transducer is simulated by the area D_T at $z=0$ and vibrates in the z direction with a strength distribution over it. With the local coordinate $\mathbf{r}'(x',y',0)$ on D_T, the scalar potential ϕ on the plane of $z=0$ is given by

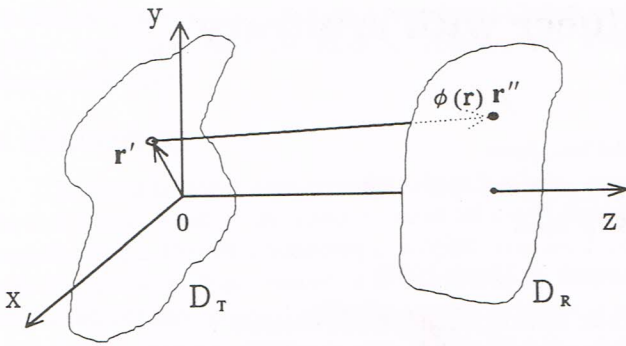$$\phi|_{z=0} = \phi_0(x',y')e^{j(\omega t - k_L z)}|_{z=0}, \quad (4)$$

FIG. 1. Ultrasonic radiation from a finite transducer.

where $\phi_0(x',y')$ assigns the strength distribution. The exact solution of Eq. (1) with the boundary condition (4) can be obtained by introducing Green's function that satisfies Eq. (4) and becomes zero on the boundary,[10] that is,

$$\phi(\mathbf{r})=\frac{e^{j\omega t}}{2\pi}\int_{D_T}\phi_0(\mathbf{r}')\left\{\frac{z}{|\mathbf{r}-\mathbf{r}'|^3}\right.$$
$$\left.+jk_L\frac{z}{|\mathbf{r}-\mathbf{r}'|^2}\right\}e^{-jk_L|\mathbf{r}-\mathbf{r}'|}\,dS_T', \qquad (5)$$

where dS_T' is a small element on D_T. The potential $\phi(\mathbf{r})$ integrates the contributions from all the elements on the radiating area to give the acoustic field at a point $\mathbf{r}$ in the medium.

For a shear wave, we assume the propagation in the z direction and the polarization in the x direction, that is,

$$\Psi_x|_{z=0}=\Psi_z|_{z=0}=0,$$
$$\Psi_y|_{z=0}=\Psi_0(x',y')e^{j(\omega t-k_T z)}|_{z=0}. \qquad (6)$$

A similar approach leads to the vector potential at a point $\mathbf{r}$,

$$\Psi_y(\mathbf{r})=\frac{e^{j\omega t}}{2\pi}\int_{D_T}\Psi_0(\mathbf{r}')\left\{\frac{z}{|\mathbf{r}-\mathbf{r}'|^3}\right.$$
$$\left.+jk_T\frac{z}{|\mathbf{r}-\mathbf{r}'|^2}\right\}e^{-jk_T|\mathbf{r}-\mathbf{r}'|}\,dS_T', \qquad (7)$$

with the prescribed strength distribution $\Psi_0(x',y')$.

B. The amplitude loss and phase shift due to diffraction

Substituting solution (5) or (7) into Eq. (3), we obtain the displacement at any point in the medium and then stresses. The amplitude loss and phase shift can be reduced from the comparison of the total stress field over the radiating area with that in a receiving one.[1] We consider the case in which the longitudinal wave from D_T is received on an area D_R, being parallel to D_T and located at a distance z from D_T (Fig. 1). Using Hooke's law represented by $\sigma_{ij}=2\mu\epsilon_{ij}+\lambda\delta_{ij}\epsilon_{kk}$, which expresses the linear relation between the stress tensor σ_{ij} and the strain tensor ϵ_{ij}, the total received pressure P_R is given by integrating σ_{zz} on D_R,

$$P_R=\int_{D_R}\left\{(\lambda+2\mu)\frac{\partial^2\phi}{\partial z^2}+\lambda\left(\frac{\partial^2\phi}{\partial x^2}+\frac{\partial^2\phi}{\partial y^2}\right)\right\}_{r=r''}\,dS_R'', \qquad (8)$$

where $\mathbf{r}''(x'',y'',z)$ is the local coordinate on D_R and dS_R'' is a small element on it. We also obtain the total input pressure P_T on D_T from Eq. (4) as

$$P_T=-k_L^2\int_{D_T}\{(\lambda+2\mu)\phi_0(x',y')e^{j(\omega t-k_L z)}\}_{r=r'}\,dS_T'. \qquad (9)$$

The ratio of their absolute values $|P_T|/|P_R|$ gives the amplitude loss L_{diff} due to the diffraction; the phase shift γ_L is given by the phase difference between the received wave and the plane wave that would propagate the distance z without suffering from the diffraction, that is,

$$L_{\text{diff}}=|P_R|/|P_T|, \qquad (10)$$
$$\gamma_L=\arg(P_R)-(\omega t-k_L z). \qquad (11)$$

For the shear-wave case, the analogous process yields the total shearing forces F_T and F_R on the radiating and receiving areas, respectively, as

$$F_T=\int_{D_T}\{k_T^2\mu\Psi_0(x',y')\}_{r=r'}\,dS_T', \qquad (12)$$

$$F_R=\int_{D_R}\mu\left\{\frac{\partial^2\Psi_y}{\partial x^2}-\frac{\partial^2\Psi_y}{\partial z^2}\right\}_{r=r''}\,dS_R'', \qquad (13)$$

and we have the amplitude loss and phase shift due to the shear-wave diffraction using a formula similar to Eqs. (10) and (11).

II. NUMERICAL METHOD FOR SOLVING POTENTIAL FIELDS

We carry out the numerical integration in Eqs. (5) and (7). The calculation consists of four steps: (i) dividing D_T and D_R into many small elements (about 3000 elements for each), (ii) calculation of the potential field generated by each element of D_T, assuming that the boundary condition (4) is satisfied on it, (iii) integration of the contributions from all the elements of D_T at an element of D_R and the integration once more of such results over D_R, and (iv) the calculation of the whole stresses on both D_T and D_R to be substituted in Eqs. (10) and (11).

We begin with the longitudinal wave. Supposing that the ith element of D_T, whose area is Δ_i and whose strength has a constant value ϕ_i over it, is located at position $\mathbf{r}_i'(x_i',y_i',0)$ as shown in Fig. 2. The boundary condition (4) becomes

$$\phi|_{z=0}=\phi_ie^{j(\omega t-k_L z)}|_{z=0}. \qquad (14)$$

From Eqs. (5) and (14), we obtain the total potential at $\mathbf{r}$ by summing up the potentials from all elements on D_T,

$$\phi(\mathbf{r})=\sum_i\frac{\Delta_i\phi_i}{2\pi}\left(\frac{z}{|\mathbf{r}-\mathbf{r}_i'|^3}+jk_L\frac{z}{|\mathbf{r}-\mathbf{r}_i'|^2}\right)e^{j(\omega t-k_L|\mathbf{r}-\mathbf{r}_i'|)}. \qquad (15)$$
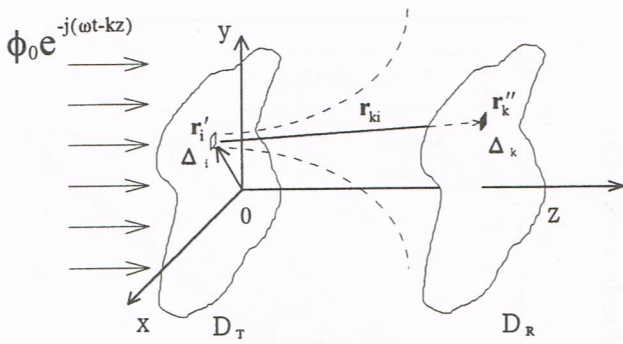
FIG. 2. Numerical integration of the acoustic field on D_R radiated from all elements on D_T.

Substituting Eq. (15) into Eq. (8) and taking the real part, the local pressure p_k operating at a receiving element Δ_k on D_R is expressed as

$$p_k = \Delta_k \sum_i \frac{\Delta_i \phi_i}{2\pi} [\tilde{A}_{ki} \cos(\omega t - k_L |\mathbf{r}_{ki}|)$$
$$- k_L \tilde{B}_{ki} \sin(\omega t - k_L |\mathbf{r}_{ki}|)], \qquad (16a)$$

where

$$\tilde{A}_{ki} = (\lambda + 2\mu) A_{ki} + \lambda C_{ki} + \lambda E_{ki},$$

$$\tilde{B}_{ki} = (\lambda + 2\mu) B_{ki} + \lambda D_{ki} + \lambda F_{ki}, \qquad (16b)$$

$$A_{ki} = \frac{15 z^3}{|\mathbf{r}_{ki}|^7} - \frac{9z}{|\mathbf{r}_{ki}|^5} + k_L^2 \left(\frac{3z}{|\mathbf{r}_{ki}|^3} - \frac{6z^3}{|\mathbf{r}_{ki}|^5} \right),$$

$$B_{ki} = \frac{15 z^3}{|\mathbf{r}_{ki}|^6} - \frac{9z}{|\mathbf{r}_{ki}|^4} - \frac{k_L^2 z^3}{|\mathbf{r}_{ki}|^4},$$

$$C_{ki} = z \left\{ \frac{15 x_{ki}^2}{|\mathbf{r}_{ki}|^7} - \frac{3}{|\mathbf{r}_{ki}|^5} + k_L^2 \left(\frac{1}{|\mathbf{r}_{ki}|^3} - \frac{6 x_{ki}^2}{|\mathbf{r}_{ki}|^5} \right) \right\},$$

$$D_{ki} = z \left\{ \frac{15 x_{ki}^2}{|\mathbf{r}_{ki}|^6} - \frac{3}{|\mathbf{r}_{ki}|^4} - \frac{k_L^2 x_{ki}^2}{|\mathbf{r}_{ki}|^4} \right\}, \qquad (16c)$$

$$E_{ki} = z \left\{ \frac{15 y_{ki}^2}{|\mathbf{r}_{ki}|^7} - \frac{3}{|\mathbf{r}_{ki}|^5} + k_L^2 \left(\frac{1}{|\mathbf{r}_{ki}|^3} - \frac{6 y_{ki}^2}{|\mathbf{r}_{ki}|^5} \right) \right\},$$

$$F_{ki} = z \left\{ \frac{15 y_{ki}^2}{|\mathbf{r}_{ki}|^6} - \frac{3}{|\mathbf{r}_{ki}|^4} - \frac{k_L^2 y_{ki}^2}{|\mathbf{r}_{ki}|^4} \right\},$$

and $\mathbf{r}_{ki} = \mathbf{r}_k'' - \mathbf{r}_i'$. We modify Eq. (16a) to

$$p_k = \Delta_k \sum_i \tilde{P}_{ki} \cos(\omega t - k_L z + \alpha_{ki})$$

$$= \Delta_k \left\{ \left(\sum_i \tilde{P}_{ki} \cos \alpha_{ki} \right) \cos(\omega t - k_L z) \right.$$

$$\left. - \left(\sum_i \tilde{P}_{ki} \sin \alpha_{ki} \right) \sin(\omega t - k_L z) \right\}$$

$$= \hat{P}_k \cos(\omega t - k_L z + \beta_k), \qquad (17a)$$

where

$$\tilde{P}_{ki} = \frac{\Delta_i \phi_i}{2\pi} \sqrt{(\tilde{A}_{ki})^2 + (k_L \tilde{B}_{ki})^2},$$

$$\qquad (17b)$$

$$\alpha_{ki} = k_L (z - |\mathbf{r}_{ki}|) + \tan^{-1} \left(\frac{K_L \tilde{B}_{ki}}{\tilde{A}_{ki}} \right),$$

$$\hat{P}_k = \Delta_k \sqrt{\left(\sum_i \tilde{P}_{ki} \cos \alpha_{ki} \right)^2 + \left(\sum_i \tilde{P}_{ki} \sin \alpha_{ki} \right)^2},$$

$$\qquad (17c)$$

$$\beta_k = \tan^{-1} \left(\frac{\sum_i \tilde{P}_{ki} \sin \alpha_{ki}}{\sum_i \tilde{P}_{ki} \cos \alpha_{ki}} \right).$$

$\hat{P}_k$ is the local amplitude on the kth receiving element and β_k is the phase. The total pressure over the receiving area is then

$$P_R = \sum_k \hat{P}_k \cos(\omega t - k_L z + \beta_k) = -\hat{P}_R \cos(\omega t - k_L z + \gamma_L),$$
$$\qquad (18a)$$

with

$$\hat{P}_R = \sqrt{\left(\sum_k \hat{P}_k \cos \beta_k \right)^2 + \left(\sum_k \hat{P}_k \sin \beta_k \right)^2},$$
$$\qquad (18b)$$

$$\gamma_L = \pi + \tan^{-1} \left(\frac{\sum_k \hat{P}_k \sin \beta_k}{\sum_k \hat{P}_k \cos \beta_k} \right).$$

representing the amplitude and phase on the whole receiving area. On the other hand, the total pressure on the source area is given by the real part of Eq. (9),

$$P_T = -\hat{P}_T \cos(\omega t - k_L z)|_{z=0},$$
$$\qquad (19)$$

$$\tilde{P}_T = \sum_i k_L^2 (\lambda + 2\mu) \phi_i \Delta_i.$$

Finally, we obtain the amplitude loss from $|\hat{P}_R|/|\hat{P}_T|$ and the phase shift from γ_L.

For the case of the shear wave, we have similar results by substituting the following equations for Eq. (16b):

$$\tilde{A}_{ki} = (-A_{ki} + C_{ki}) \mu,$$
$$\qquad (20)$$
$$\tilde{B}_{ki} = (-B_{ki} + D_{ki}) \mu.$$

III. RESULTS OF NUMERICAL COMPUTATION

We suppose the same transducer for the generation and reception throughout the calculation, because many ultrasonic measurements are conducted using a transducer in the reflection mode and the ultrasonic wave launched from a transducer is received by the same one after reflections. We calculate the amplitude loss and phase shift for the three cases: (i) the near field, where the wavelength is not necessarily small relative to the propagation distance, (ii) a rectangular transducer shape, and (iii) a circular transducer with a strength distribution. A set of numerals used is taken for steel: $C_L = 5900$ m/s, $C_T = 3200$ m/s, $\rho = 7850$ kg/m^3, $\lambda = 117$ GPa, and $\mu = 80.0$ GPa.

A. Effects of the near field

For the far-field receiving, the propagation distance z is large enough relative to the wavelength Λ, that is, $k|\mathbf{r}| \gg 1$

and $|\mathbf{r}| \approx z$. The first terms in the integrands in Eqs. (5) and (7) can then be neglected relative to the second terms. The potential ϕ is then approximated by the expression

$$\phi(\mathbf{r}) = jk_L \frac{\phi_0 e^{j\omega t}}{2\pi} \int_{D_T} \frac{e^{-jk_L|\mathbf{r}-\mathbf{r}'|}}{|\mathbf{r}-\mathbf{r}'|} dS_T'. \quad (21)$$

The same expression holds for the shear wave with ϕ replaced by ψ_y and k_L replaced by k_T. Equation (21) was derived by Rayleigh[8] and has been the basis of the previous work on the diffraction calculation. It represents the acoustic potential in the medium, which is obtained by integrating the radiation from the elements on D_T vibrating with the constant strength ϕ_0. Each radiation decays at a rate proportional to the wavelength times the propagation distance and possesses the phase of $(\omega t - k_L|\mathbf{r}-\mathbf{r}'|)$ plus a constant advance of $\pi/2$. Figure 3 compares the exact solutions [Eqs. (5) and (7)] and the Rayleigh integral [Eq. (21)] for the circular transducer with a uniform strength over the aperture. The horizontal axis $S = (\Lambda z)/a^2$ is the nondimensional parameter,[1] which governs the diffraction phenomena; a is the transducer radius and z the propagation distance. When $\Lambda/z \ll 1$, the exact solutions yield practically the same diffraction loss for the longitudinal and shear waves, which are well approximated by Eq. (21). However, if Λ and z are comparable with each other, the longitudinal and shear waves undergo different diffraction loss, which Eq. (21) fails to describe. Rayleigh's approximate expression is, of course, inapplicable for discussing such a near-field diffraction behavior and we have to deal with the longitudinal and shear waves separately, relying on Eqs. (5) and (7). We see no significant difference on the phase shift, which is asymptotic to $\pi/2$ as S increases in all cases.
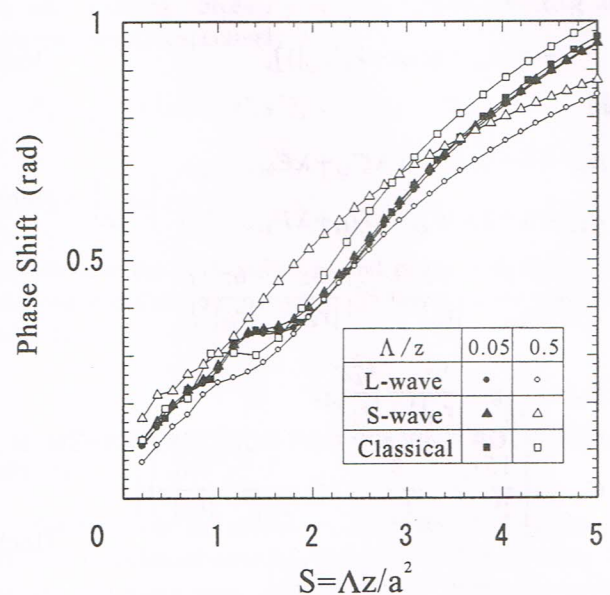
The far field is not clearly bounded from the near field because the diffraction nature changes gradually from one extreme to another. The present calculations indicate that the far field is found in the order of $\Lambda/z < 10^{-3}$.

B. Effects of transducer geometry

When the transducer has a noncircular shape, the amplitude loss will be larger than the circular case, since the transducer is more likely to miss the reflected echoes. We consider rectangular transducers having the various ratios of the width and the height (w/h) with a uniform strength. In Fig. 4, the horizontal axis S is defined by using the equivalent radius whose circular area equals the rectangular one ($a = \sqrt{wh/\pi}$). For comparison purposes, it contains the Seki et al. result for the circular case. Since we performed the calculations in the far field, we have the same results for longitudinal and shear waves. For the square transducer ($w/h = 1$), both loss and phase shift are almost the same as the circular case. But, as the shape is apart from being circular, the effects are progressively enhanced in magnitude. Especially in the region of $w/h > 1.5$, they show a significant difference from the circular case, indicating that the result of Seki et al. is no longer useful for the diffraction correction even if the equivalent area is involved. We have to use the diffraction data specific to each transducer geometry.
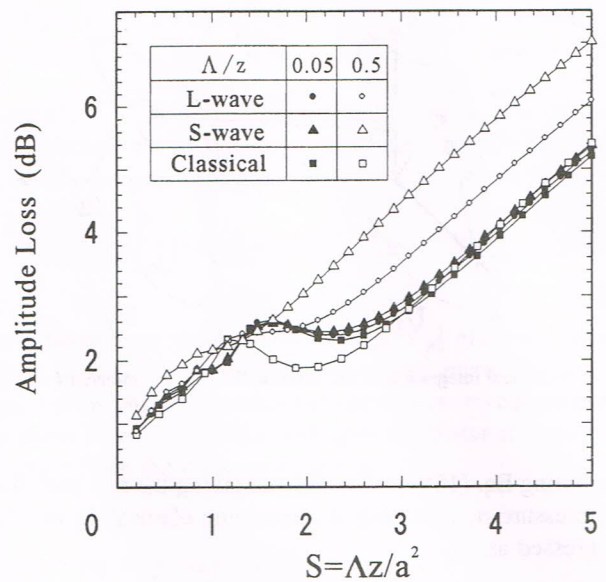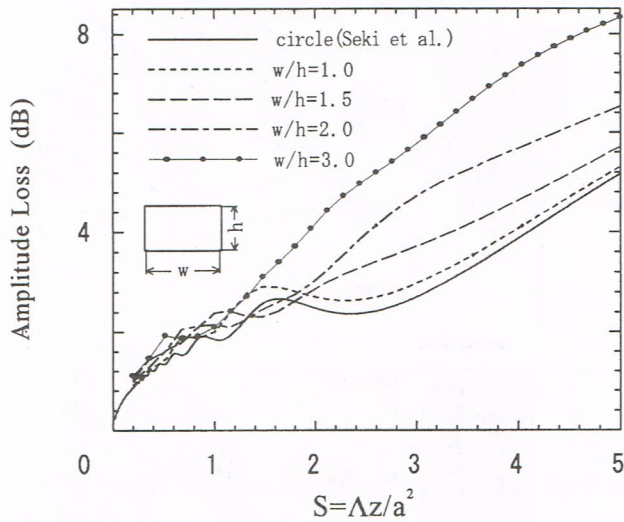
(a) amplitude loss

(b) phase shift

FIG. 3. Comparison of the diffraction effects among longitudinal waves, shear waves, and classical solution in the near fields. Classical solution is based on Rayleigh's approximate integration. The horizontal axis is a nondimensional distance parameter; Λ is the wavelength, z the propagation distance, and a the transducer radius.

C. Effects of strength distribution on the radiating area

We calculated the diffraction effect for the circular transducer in the far field [Eq. (21)], but with a strength distribution on both D_T and D_R. The distributions considered are the Gaussian profile and a parabolic profile, in which the intensities along the edges are a part of tenth of the maxima at the centers. The maximum sensitivity at the center of D_R is determined so that the amplitude loss becomes zero at $S = 0$, which is a natural consequence of the diffraction effect. Figure 5 presents the results along with the classical solution[1]
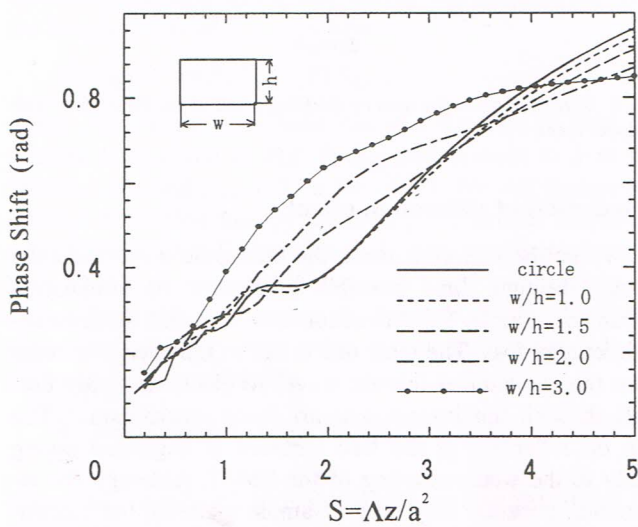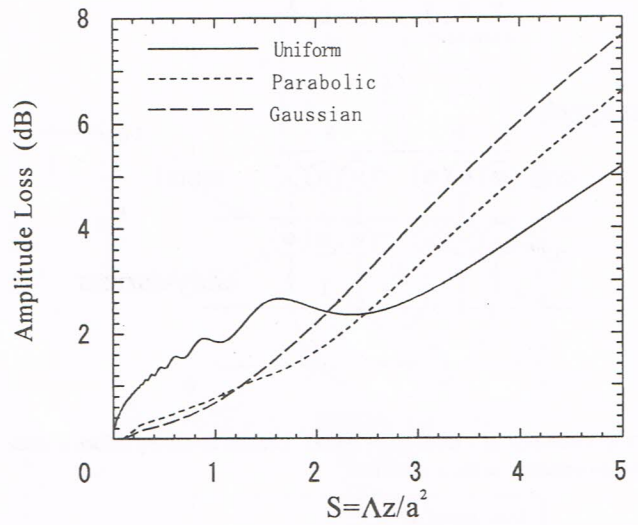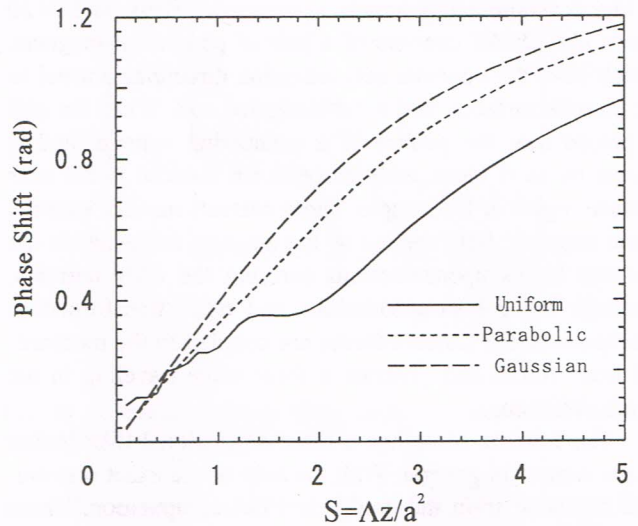
FIG. 4. Diffraction effects for rectangular transducers. a is the transducer radius for the circle case and equals $\sqrt{wh/\pi}$ for the rectangular cases; w and h are width and height of the transducer area.

FIG. 5. Diffraction effects for a transducer having the Gaussian or a parabolic distribution on the radiation and receiving areas. a is the transducer radius.

for the uniform strength over the area.

Such a centered strength of transduction alters the received amplitude in a peculiar way through two conflicting mechanisms. On the sending side, the acoustic field is mainly radiated by the center part. Even if the ultrasonic beam spreads, the receiving transducer will detect the major part of it, inducing less diffraction loss than the uniform strength. On the receiving side, however, the transducer is insensitive to the waves impinging the edge part. This situation is equivalent to receiving the wave with a small transducer and then more diffraction loss arises. These positive and negative effects are present in Fig. 5(a). When S is small enough, the wave field does not diffract wide before arriving at the receiver and the positive effect dominates the negative one. When S is large and the transducers are separated, the diffraction occurs to a substantial extent and the transducer picks up only the middle part, decreasing the received am-

plitude. The difference in the phase shift [Fig. 5(b)] can be explained by approximating the transducer by the point source and the point receiver. In this case, $\mathbf{r}'$ in the integrand of Eq. (21) becomes zero and $\phi(\mathbf{r})$ has a phase of $(\omega t - kz + \pi/2)$, that is, the maximum possible phase change of $\pi/2$ relative to the plane wave. The centered strength then induces a larger phase shift than the even strength. It is clear that these tendencies are more remarkable for the Gaussian profile than for the parabolic profile, because the Gaussian profile has a sharper concentration of the intensity around the center.

IV. APPLICATION TO THE EMAT EXPERIMENT

A. Modeling for the EMAT

We applied the calculated results to the diffraction phenomena observed with a shear-wave electromagnetic acous-
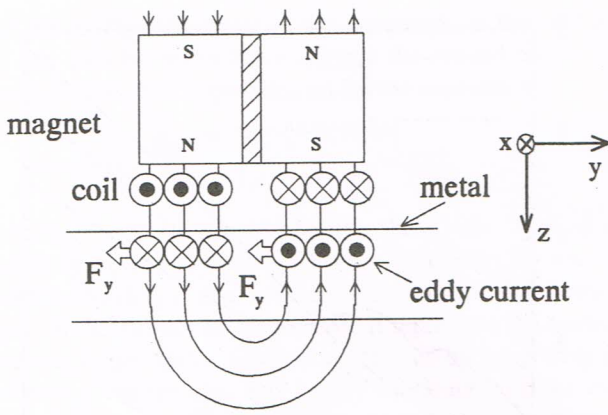
FIG. 6. Operation of a shear-wave EMAT. Lorentz forces F_y induce a shear wave propagating in the z direction.

tic transducer (EMAT). The EMAT is schematically sketched in Fig. 6, whose active area is a rectangular shape of 14×20 mm². The EMAT consists of a pair of permanent magnets, which have the opposite magnetization directions normal to the sample surfaces, and a flat elongated coil. When the coil is placed near the surface of a conducting material and is driven by an rf burst, eddy currents are induced in the near surface region of the sample. These currents interact with the static magnetic field applied by the magnets and generate the Lorentz forces upon electrons carrying the eddy currents. Through the collision with ions and other transformation mechanisms, the Lorentz forces are coupled to the mechanical body forces and generate a shear wave traveling in the depth direction.

The Lorentz force has a three-dimensional distribution in the sample in general. With the help of the exact distribution available from the nonlinear FEM computation,[11] here we simplify the distribution to be two dimensional on the sample surface, which is characterized by a pair of parabolic curves (Fig. 7). (The eddy current by the coil and the static magnetic field due to the permanent magnets are separately calculated to obtain the Lorentz force in the surface region.) This simplification is allowable when the sample has a good electric conductivity and a high permeability because such a material has a very small electromagnetic skin depth, confining the Lorentz forces in the surface region.
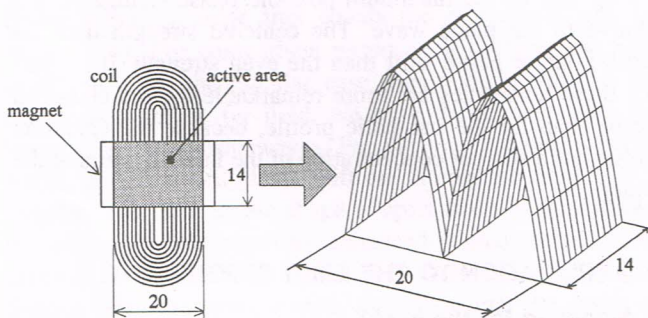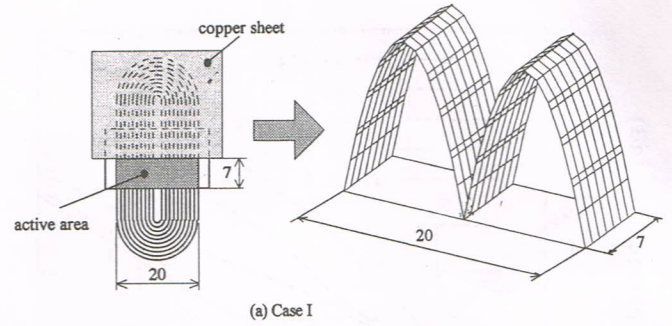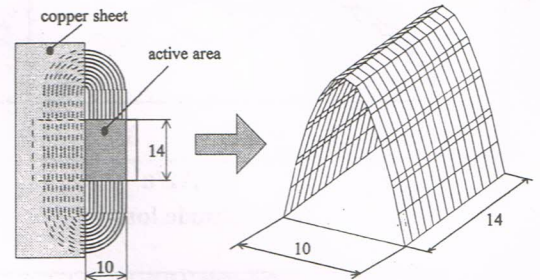

FIG. 7. Approximation of the Lorentz force distribution by a pair of parabolic curves (unshielded case).

(a) Case I

(b) Case II

FIG. 8. Change of the active area by shielding a half of the EMAT face with a copper sheet.

B. Isolation of diffraction effect

When the EMAT is used, the ultrasonic wave loses the energy through three possible processes: (i) attenuation within the sample, (ii) diffraction loss, and (iii) electromagnetic energy loss. The third one refers to the energy transfer from the mechanical (elastic wave) to electrical (eddy current) through the inverse Lorentz force mechanism.[12] The loss on reflecting at the free surfaces is neglected owing partly to the weak coupling of the EMAT. Although the attenuation depends only on the sample material, the electromagnetic energy loss depends not only on the material property but also on the static magnetic field. To isolate the diffraction effect and verify the numerical calculation, we produced two different radiating geometries by shielding half of the EMAT face with a copper sheet (0.045 mm thick) in two ways, thereby suppressing the eddy currents there to make this part inactive. The sample was unchanged. We compared the received echo amplitudes for these transducer geometries in the reflection experiments. Case I has an active area of 7×20 mm² with double parabolic profiles and case II has a 14×10 mm² area with a single parabolic profile, as illustrated in Fig. 8. Both cases contain the same static magnetic field so that the same amount of the electromagnetic loss will occur. The amplitude losses calculated for the two cases are presented in Fig. 9 together with the unshielded response.

In the pulse-echo measurement for case I, the ratio of the amplitude A_n of the nth echo to A_i of the ith echo ($n > i$) is written as

$$\tilde{A}_n^i \equiv A_n / A_i = D_n^i e^{-2L(n-i)(\alpha + \alpha_e)}, \tag{22}$$

where α is the attenuation coefficient, α_e the electromagnetic energy loss, and L the sample thickness. Because D_n^i solely
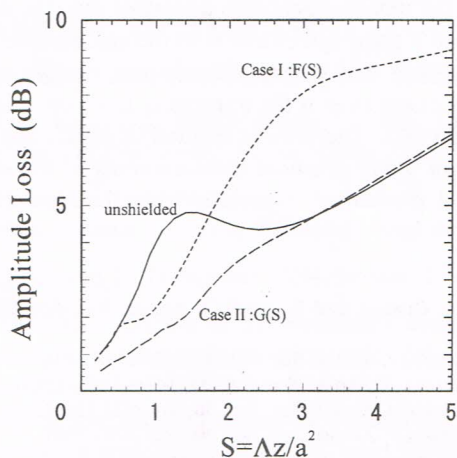
FIG. 9. Amplitude losses due to the diffraction for unshielded EMAT, case I, and case II.

represents the diffraction loss during the propagation over the length of $2L(n-i)$, it satisfies

$$20 \log(D_n^i) = F(S_{Ai}) - F(S_{An}), \tag{23}$$

where $F(S)$ is the amplitude loss as a function of Seki parameter S as given in Fig. 9; S_{Ai} corresponds to S at the distance $2Li$ and S_{An} to $2Ln$ for case I. We can discuss the relative diffraction loss by measuring the similar amplitude ratio $\tilde{B}_n^i$ with case II, because α, L, and α_e are common to both EMAT geometries for the same i and n. The ratio $\tilde{A}_n^i$ differs from the counterpart $\tilde{B}_n^i$ because of the dissimilar transducer geometry with other parameters unchanged; we have the following relation:

$$20 \log(\tilde{B}_n^i/\tilde{A}_n^i) = \{F(S_i) - G(S_i)\} - \{F(S_n) - G(S_n)\}, \tag{24}$$

where the function $G(S)$ is the amplitude loss calculated for case II. Namely, the quantity in Eq. (24) depends only on the propagation geometry in the sample, isolating the diffraction effect.

C. Experimental result

The sample was a plate of fine-grained alloy steel 25 mm thick ($100^l \times 100^w \times 25^t$). The echo amplitudes, up to the 15th reflection, were measured by driving the EMAT (case I, case II, and unshielded) with high-power rf bursts of 5-μs duration, employing the superheterodyne process for the received echo signals, and integrating the outputs with an integrator gate 10 μs wide.[13] The operation frequencies were 3 and 6 MHz. The echo amplitudes were normalized by the second echo amplitude, that is, $i=2$. The first echo was useless since it was partially overlapped by the tail of the exciting signal.

Figure 10 shows the normalized amplitudes for the three cases. At the 6-MHz measurements, the amplitude ratios for case II are larger than those for the unshielded case in spite of the smaller area (or larger Seki parameter). This occurs because the geometry for case II has a strength concentration around the centerline, which decreases the diffraction loss as discussed above. Figure 11 summarizes the relative diffrac-
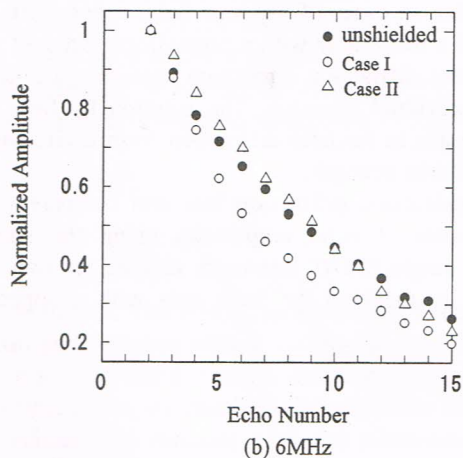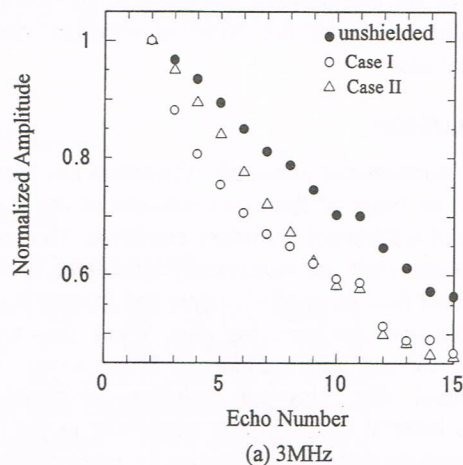

(a) 3MHz

(b) 6MHz

FIG. 10. Normalized amplitude by the second echo amplitude for each of unshielded EMAT, case I, and case II.

tion loss between cases I and II from Eq. (24). The solid line is obtained from the numerical data for these geometries. The measurements at the frequency of 6 MHz are very favorably compared with the calculation. But the comparison is not so good for 3 MHz. This discrepancy can be ascribed to a thicker electromagnetic skin depth associated with lower frequencies, which makes the Lorentz force excitation deeper from the sample surface. For the lower frequencies, the sim-
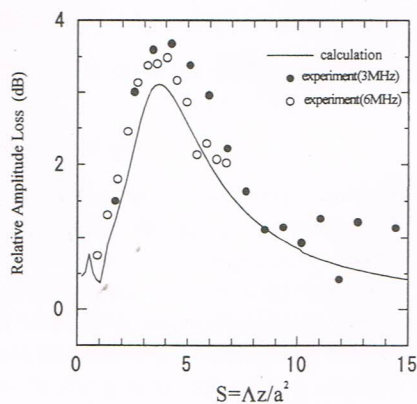

FIG. 11. Comparison of the relative amplitude loss between the calculation and the experiments. $a = \sqrt{wh/\pi}$, where w and h are width and height of the active area of the EMAT.

plification of the two-dimensional strength distribution is no longer valid and then we have to consider the three-dimensional case.

V. CONCLUSION

Three-dimensional ultrasonic diffraction has been investigated on the basis of the exact solution of the Helmholtz equation and a Dirichlet boundary condition. The amplitude loss and phase shift are numerically calculated by dividing the transducer face to small elements and integrating the potential fields over the receiving area. While the exact solutions, both for the longitudinal and shear waves, approximately equal the classical solution obtainable from Rayleigh's integral for a circular transducer in the far field, they demonstrate different tendencies for more general cases. In particular, in cases of the near field, a noncircular transducer, and a transducer with a nonuniform strength over the aperture, the diffraction correction requires calculated data for the individual situation. The solution by Seki et al. is limited to use in far-field diffraction from a circular source with a uniform strength.

The calculated diffraction loss was compared with the measurements of echo amplitudes using the shear-wave EMAT. A single EMAT was used, making the two different apertures by masking the front area with a copper sheet. Although the measurement was a relative one, the amplitude loss showed a good agreement with the calculation. With the diffraction data thus calculated, one can easily correct the diffraction errors even if the transducer has a complex geometry like EMATs. The present method of diffraction analysis is useful for many practical measurements of ultrasonic velocities and attenuation, especially when the high accuracy is required.

[1] H. Seki, A. Granato, and R. Truell, J. Acoust. Soc. Am. **28**, 230–238 (1955).
[2] E. P. Papadakis, J. Acoust. Soc. Am. **31**, 150–153 (1959).
[3] H. J. McSkimin, J. Acoust. Soc. Am. **32**, 1401–1404 (1960).
[4] E. P. Papadakis, J. Acoust. Soc. Am. **36**, 414–422 (1964).
[5] E. P. Papadakis, J. Acoust. Soc. Am. **40**, 863–876 (1966).
[6] K. Beissner, Acoustica **49**, 212–217 (1981).
[7] X. M. Tang, M. N. Toksoz, and C. H. Cheng, J. Acoust. Soc. Am. **87**, 1894–1902 (1990).
[8] L. Rayleigh, *The Theory of Sound II* (Dover, New York, 1945), p. 107.
[9] J. D. Achenbach, *Wave Propagation in Elastic Solids* (Elsevier, New York, 1973), p. 86.
[10] R. K. Luneburg, *Mathematical Theory of Optics* (University of California, Berkeley, 1966), p. 311.
[11] H. Ogi, M. Hirao, K. Minoura, and H. Fukuoka (to be submitted).
[12] H. Ogi, M. Hirao, T. Honda, and H. Fukuoka, *Review of Progress in Quantitative NDE*, 14, edited by D. O. Thompsin and D. E. Chimenti, pp. 1601–1608 (1995).
[13] M. Hirao, H. Ogi, and H. Fukuoka, Rev. Sci. Instrum. **64**, 3198–3205 (1993).